Article

Reduction of Cogging Torque in Surface Mounted Permanent Magnet Brushless DC Motor by Adapting Rotor Magnetic Displacement

T. A. Anuja and M. Arun Noyal Doss *

Department of Electrical and Electronics Engineering, SRM Institute of Science and Technology, SRM Nagar, Kattankulathur 603203, India; taanuja@gmail.com
* Correspondence: arunnoyal@gmail.com or arunoyad@srmist.edu.in

Abstract: Cogging torque is a critical dilemma in Permanent Magnet Brushless DC (PMBLDC) motors. In medium-low power PMBLDC motors, redundant vibrations and forbidding noises arise as a result of the harmonic magnetic forces created by cogging torque. This paper introduces a simple approach for minimizing cogging torque in PMBLDC motors by applying placement irregularities in rotor magnets. An angle shift in the rotor magnets in surface-mounted PMBLDC motors helps to attain magnet displacement. This displacement imparts an asymmetrical magnet structure to the rotor. Maintaining pole arc to pole pitch ratio (L/τ) of between 0.6 and 0.8, shifting angles from $1°$ to $8°$ were considered in order to analyze the effect of the angle shift on the rotor magnets. An analytical expression was also derived for finding the shifting angle with the minimum cogging torque in the PMBLDC motor by using the Virtual Work Method (VWM). The optimization of the shifting angle with minimum cogging torque was investigated using 3D Finite Element Analysis (FEA). A comparison of the simulation and analytical results of cogging torque was carried out. It was determined that the reduction of cogging torque in the analytical results showed good agreement with the FEA analysis.

Keywords: PMBLDC motor; cogging torque; finite element analysis; virtual work method; shifting angle

1. Introduction

Permanent Magnet Brushless DC (PMBLDC) motors are machines with excellent torque–speed characteristics, excellent efficiency, and nominal maintenance cost. They are very favorable for unidirectional variable-speed applications such as automotive pumps and fans [1]. They are also very supportive with respect to achieving compactness in terms of machine size [2]. They produce a negligible amount of electromagnetic and mechanical noise. They also exhibit excellent durability due to their lack of mechanical contact [3]. One of the great flaws in the BLDC motor is its torque ripple, which is built into the design [4]. One of the main reasons for torque ripple is cogging torque. Cogging torque also generates enormous, troubling noise and shaking movements in the machine itself, as well as in its load. For this reason, cogging torque reduction methods play a vital role in PMBLDC motor design. Generally, cogging torque derives from motors using permanent magnets such as Permanent Magnet Brushless DC (PMBLDC) motors and permanent Magnet Synchronous motors. The root cause for the generation of cogging torque in BLDC motors is the magnetic interaction between the permanent magnet and the steel in the slotted armature. A lot of techniques are currently available for the minimization of cogging torque in BLDC motors. Nowadays, BLDC motors are used in rigorous applications such as electric power steering, robotics, etc. Hence the reduction of cogging torque has come to be a grueling task.

Over the last two decades, numerous studies have been conducted on the cogging torque of PMBLDC motors. These methods have included electromagnetic methods and

mechanical methods. The authors recommended a core skew structure for reducing the
cogging torque in [5]. When applying this property, no-load THD and the fifth and seventh
harmonics were the main harmonic components of the back-EMF. However, when skewing
the core, some residual magnetism is lost. Modification of the machine's magnetic circuit
resulted in the occurrence of additional harmonics in the cogging torque in [6]. They
focused on a symmetrical rotor with an asymmetrical stator or an asymmetrical rotor with
a symmetrical stator. Nonlinear algorithms were proposed for the reduction of cogging
torque in [7–9]. A feedback linearization strategy was used in [7], mathematical modeling
of cogging torque phenomena was performed in [8], and field-oriented control operations
were used in [9]. A new technique for radial flux surface-mounted PMBLDC motors was
proposed by applying T-shaped bifurcations in the stator teeth in [10]. However, this
reduced the mechanical strength of the stator. In order to reduce the cogging torque,
the slot was closed by a sliding separator in [11]. For small-sized machines, it is very
difficult to place a slider inside the slot. The authors recommended notches in the rotor
in [12]. However, adding notches in the rotor side is a tedious mechanical process. A new
technique in the winding side was proposed in [13]. Coil winding concentrated on the
phase group is a good solution for cogging torque reduction, but increases the complexity
of the winding. Magnet step skewing and reduction of the claw pole width was carried
out in a claw pole machine in [14]. Magnet step skewing causes a reduction in residual
magnetism and the unequal width in the claw pole increases the structural complexity.
U-clamped magnetic poles were recommended for the reduction of cogging torque and
even flux per pole in [15], so a machine with a greater number of slots is recommended,
as well as a high magnet thickness. In [16], a novel air gap profile was introduced for
a single-phase PMBLDC motor. This air gap profile consists of a dip and a dip angle.
By varying the dip and dip angle, a handful of air gap profiles could be generated, and
profiles with a dip angle less than the critical dip angle exhibited improved starting torque
by up to 70%. In [17], the reduction of cogging torque and acoustic noise in permanent
magnet motors with larger stator slot openings was investigated. Here also, tooth pairings
with two different types of tooth width were proposed. The experimental results showed
that the proposed tooth pairings reduced cogging torque by 85% and acoustic noise by
3.1 dB. Reference [1] showed how to minimize high cogging torque without increasing the
manufacturing cost. A systematic means was presented by which the selected introduction
of auxiliary slots can double the fundamental frequency of the cogging torque, making
stator claw skewing much more effective at reducing cogging torque; both measures can
feasibly be carried out at the stage of punching the steel sheets and their subsequent deep
drawing, at no additional cost. Reference [18] reported a stator shape optimization design
for reducing the cogging torque of single-phase brushless DC (BLDC) motors by adopting
an asymmetrical airgap to make them self-start. A model that combined Latin hypercube
sampling and a genetic algorithm was used to reduce the cogging torque and maintain
the efficiency and torque. As an optimal design result, the cogging torque of the optimal
model decreased. Ref. [19] proposed a new design of SPOKE-type PM brushless direct
current (BLDC) motor without using neodymium PM (Nd-PM). The proposed model had
an improved output characteristic, as it used the properties of the magnetic flux effect of the
SPOKE-type motor with an additional pushing assistant magnet and sub assistant magnet
in the shape of a spoke. In this paper, ferrite PM (Fe-PM) was used instead of Nd-PM. The
authors of [20] introduced a genetic algorithm for optimal core shape design for reducing
cogging torque in brushless DC motors used in digital versatile disk drive systems or hard
disk drive systems. The optimized or rounded core could be a recommended core shape
for the outer-rotor-type BLDC motor for a DVD ROM drive system in order to achieve
low cogging torque. Ref. [21] described a novel rotor pole shape consisting of a uniform
surface and an eccentric surface, leading to a sinusoidal magnetic flux density in the air gap
and reducing cogging torque, torque ripple, and the harmonics of the back-electromotive
force waveform in a spoke-type brushless DC motor. This novel rotor included an eccentric
surface. The proposed method had a smooth variation of reluctance, producing a near

sinusoidal magnetic flux waveform in the air gap. This caused a reduction in the losses between the upper edge of the permanent magnet and the adjacent stator teeth, and an increment of the effective flux by concentrating the flux. Ref. [22] proposed an anisotropic ferrite magnet shape and magnetization direction to maximize back-EMF in an IPM BLDC motor. Firstly, four different models of general magnet shapes were selected, and then FEM analysis was carried out using four different magnetization directions for each of the four models. The best magnet shape and magnetization direction for each model was used to determine an initial model for optimization. Secondly, based on the initial model, optimization design for maximum back-EMF and minimum cogging torque and THD was performed. Reference [23] presented the stator and rotor shape designs for an interior-permanent magnet (IPM)-type brushless DC (BLDC) motor for reducing torque fluctuation. A partly enlarged air gap is introduced by the unequal diameter of the rotor and core structure of the stator with pole shoe modification. A reduction in torque ripple was obtained by upgrading the torque value at the minimum torque position, and their detail characteristics were compared. The addition of holes in the rotor core is a better solution for overcoming this problem. The additional torque fluctuation was decreased.

In the context of the exploration of different cogging torque reduction methods, motors with asymmetrical magnets represent a productive technique. This paper introduces a novel design based on an asymmetrical rotor structure by applying a shifting angle to the PM. The shifting angle method is not a skewing method, where the skew technique is used for skewing the rotor PMs. The shifting angle method alters the position of the permanent magnet by changing the pole pitch. To analyze the effect of magnets shifting in the BLDC motor, 3D-FEA analysis and numerical analysis were performed. To study the impact of varying the angle between the permanent magnet on the rotor, a range of different angles were considered. The rotor permanent magnet was shifted from 1° to 8°. To effectively decrease the cogging torque, an optimal 3° shift to the permanent magnet (AB-87°, BC-87°, CD-93°, and DA-93°) was determined. The resulting design also obtained the correct trapezoidal shape of the back-EMF. Compared to the reference model, it was able to achieve a 60% reduction in cogging torque. This method is able to achieve excellent performance characteristics. The simulation results were compared with the analytical results, and the reduction of cogging torque in the two analyses was almost the same.

The organization of the paper is as follows: the design of the BLDC motor is presented in Section 2. The analytical expression of cogging torque by VWM is presented in Section 3. Finite element analysis of the symmetrical rotor is presented in Section 4. The effect of the angle shift on cogging torque is shown in Section 5.

2. Design of BLDC Motor

The basic step in the motor design is to fix the rated speed and torque. Based on these particulars, the other parameters of the motor can be selected. Figure 1 shows the structure of a surface-mounted PMBLDC motor.

The stators of BLDC motors are similar to those of three-phase induction motors. The main dimensions depend on the specific electric loading and specific magnetic loading. The procedure for calculating the main dimensions is depicted as a flowchart in Figure 2. The procedure for the selection of stator slots and winding is shown in Figure 3.

In this paper, in order to analyze cogging torque reduction, a 4-pole, 12-slot surface-mounted BLDC motor was used. The design parameters of the motor are shown in Table 1.
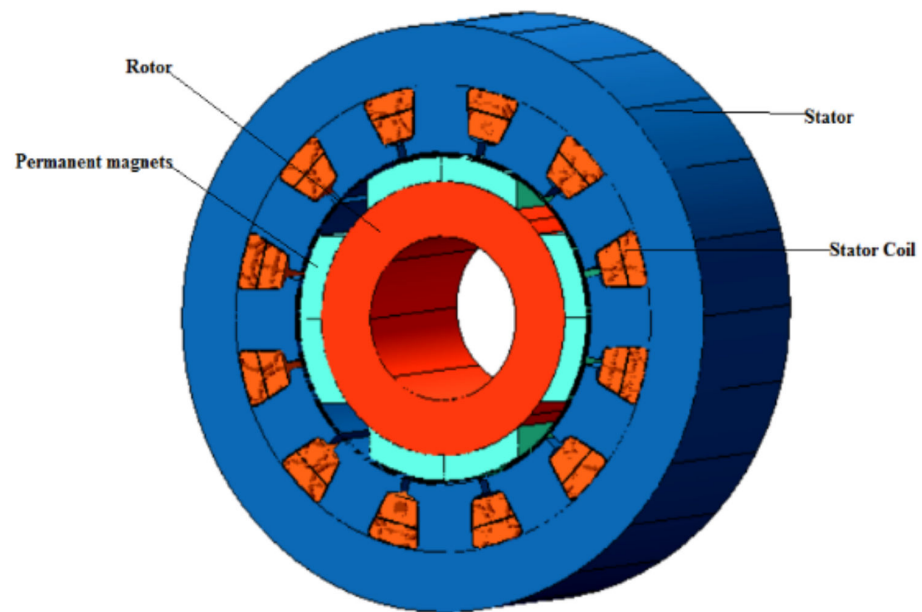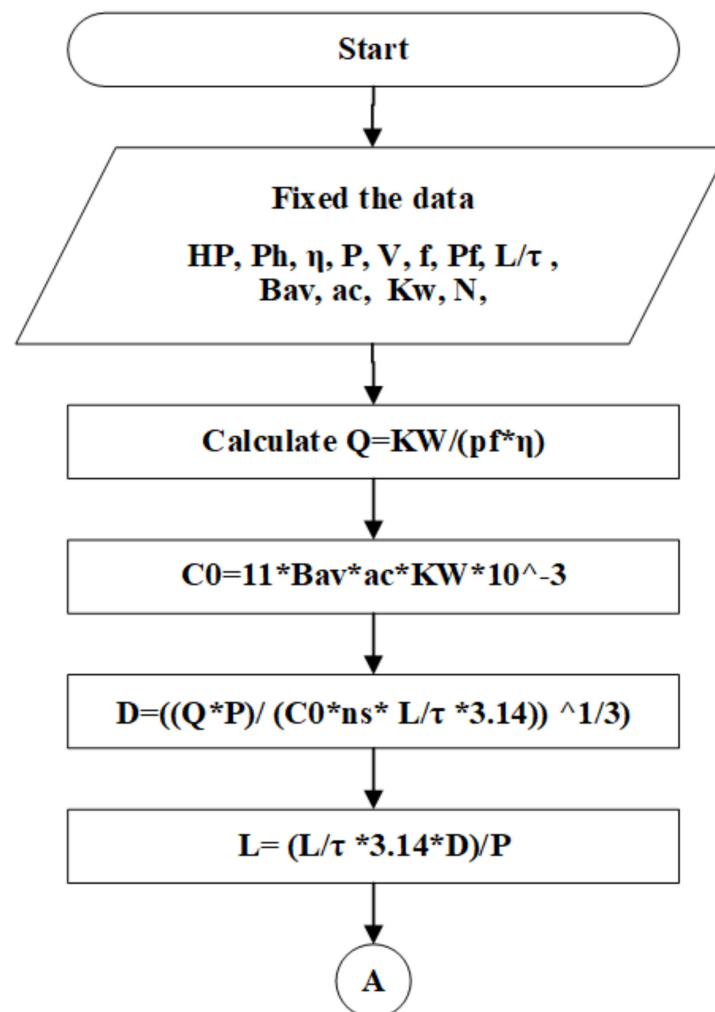
Figure 1. Topology of surface-mounted BLDC motor.

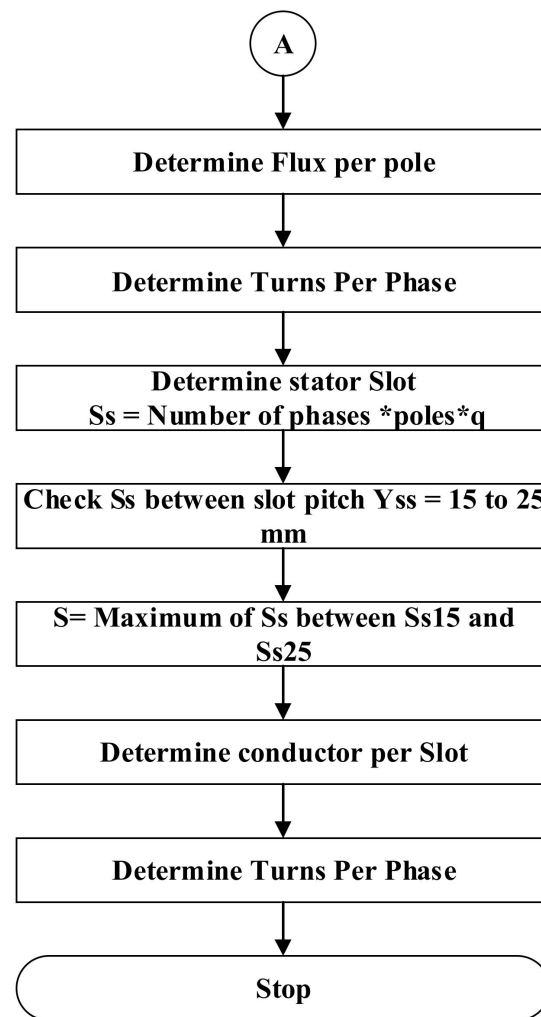
Figure 2. Flowchart for calculation of main stator dimensions.

Figure 3. Flowchart for stator slots and windings.

Table 1. Design parameters.

Parameters	Rating	Parameters	Rating
Supply Voltage (v)	48	Power (HP)	1
Number of poles	4	Number of Slots	12
Rated Speed (rpm)	5000	Inner Diameter Rotor (mm)	16.7
Outer Diameter (mm)	60	Outer Diameter Rotor (mm)	33
Stack Height (mm)	50	Airgap Thickness (mm)	0.5
Pole Arc	63°	Magnet Thickness (mm)	2.5

3. Analytical Expression of Cogging Torque by VWM

The most widely used method for calculating cogging torque is the virtual work method (VWM). The virtual work method is also called the co-energy method [24]. The basic principle is that neglecting the variation in magnets and iron of PMBLDC motor, the cogging torque of an ideal lossless PMBLDC motor can be expressed as the derivative of co-energy in the air gap [25]. According to [26], cogging torque is produced because of the interaction between the PMs and the armature and the slot. Because of this interaction in the absence of a current, energy variation occurs inside the motor.

$$E_v = E_{v.I} + E_{v.airgap} + E_{v.PM} \tag{1}$$

where E_v is the total energy variation, $E_{v.I}$ is the energy variation in iron, $E_{v.airgap}$ is the energy variation in airgap, and $E_{v.PM}$ is the energy variation in PM.

When compared with the energy variation in the airgap and PM, only a minor variation occurs in iron. Therefore

$$E_v \cong E_{v.airgap} + E_{v.PM} = \frac{1}{2\mu_0} \int \int \int B^2 dv \tag{2}$$

Hence, cogging torque can be stated as

$$T_{cog} = -\frac{\partial E_v}{\partial \propto} \tag{3}$$

where, μ_0, B and $\propto$ are the permeability of air, the magnetic flux density (magnetic induction) and the angle of rotation of the rotor, respectively. The distribution of magnetic induction certainly stated as

$$B\,(\theta, \alpha) = B_{rs}(\theta) \frac{l_m}{l_m + lg(\theta, \alpha)} \tag{4}$$

where $B_{rs}(\theta)$ is the residual flux density along the periphery of the airgap, l_m is the length of the permanent magnet, and l_g is the effective length of airgap distribution. Equation (2) can be redrafted as

$$E_v = \frac{1}{2\mu_0} \int \int \int B_{rs}{}^2(\theta) \left[\frac{l_m}{l_m + lg(\theta, \alpha)} \right]^2 dv \tag{5}$$

To obtain the magnetostatic energy within the motor, Fourier expansion of $B_{rs}{}^2(\theta)$ and $\left[\frac{l_m}{l_m + lg(\theta, \alpha)} \right]^2$ can be performed.

$$B_{rs}{}^2(\theta) = B_{rs0} + \sum_{n=1}^{\infty} B_{rsan}cosn\theta + B_{rsbn}sin\,n\,\theta \tag{6}$$

$$\left[\frac{l_m}{l_m + lg(\theta, \alpha)} \right]^2 = G_0 + \sum_{n=1}^{\infty} G_n cos\,n\,s\,(\theta + \alpha) \tag{7}$$

The analytical statement of cogging torque for asymmetrical magnets can be expressed as

$$T_{cog} = \frac{\pi z Ls}{4\mu_0} \left(R_r^2 - R_s^2 \right) \sum_{n=1}^{\infty} B_{rsanz}sin\,n\,s\,\alpha + B_{rsbnz}cos\,n\,s\,\alpha \tag{8}$$

where Ls is the length of the stack, s is the slot number, Rr is the rotor outer radius and Rs is the stator inner radius. The Fourier coefficients B_{rsanz} and B_{rsbnz} can be expressed as

$$B_{rsanz} = \frac{2B_{rs}^2}{ns\pi} sin\,\frac{ns\pi\alpha_p}{2p} \sum_{k=1}^{2p} cos\,ns\left[\frac{\pi}{p}(k-1) + \theta_s \right] \tag{9}$$

$$B_{rsbnz} = \frac{2B_{rs}^2}{ns\pi} sin\,\frac{ns\pi\alpha_p}{2p} \sum_{k=1}^{2p} sin\,n\,s\left[\frac{\pi}{p}(k-1) + \theta_s \right] \tag{10}$$

where, θ_s is the shifting angle.

When symmetrical structure is adopted for the magnets ($\theta_s = 0°$), B_{rsbnz} is zero and cogging torque can be expressed as

$$T_{cog} = \frac{\pi z Ls}{4\mu_0} (R_r^2 - R_s^2) \sum_{n=1}^{\infty} B_{rsanz}sin\,n\,s\,\alpha \tag{11}$$

Table 2 shows the analytical results of cogging torque with shifting angles ranging from 1° to 8°. Figure 4 shows a graphical representation of cogging torque with shifting angles ranging from 1° to 8°.

Table 2. Analytical results for cogging torque with shifting angles from 1° to 8°.

Shifting Angle (°)	1	2	3	4	5	6	7	8
Cogging torque (Nm)	0.39	0.3	0.15	0.18	0.45	0.2	0.6	0.51
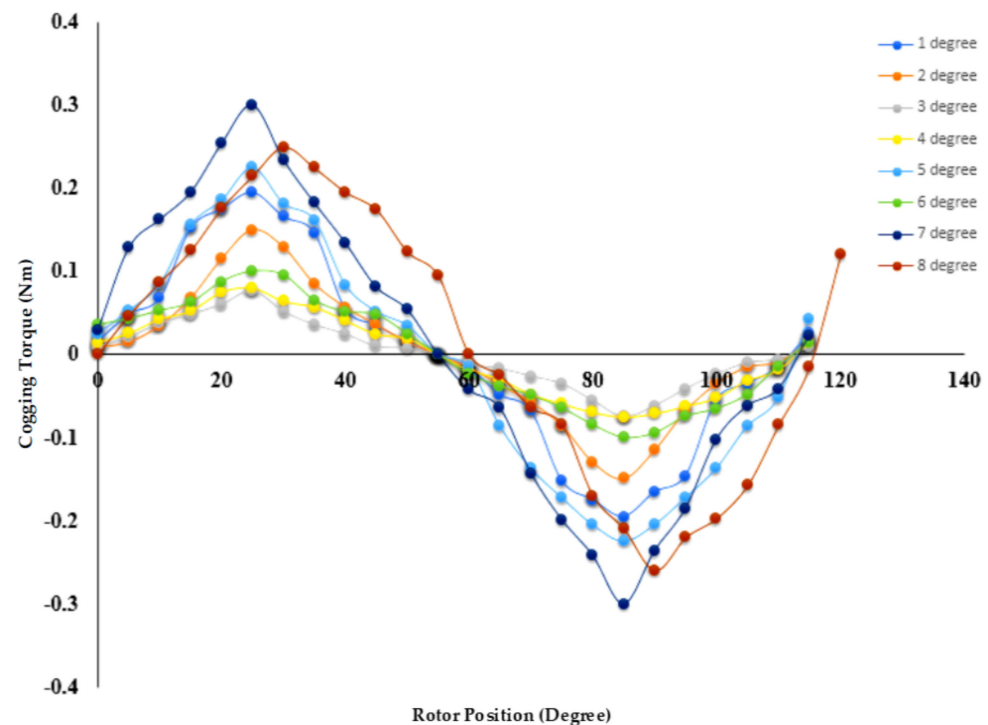
Figure 4. Analytical results of cogging torque with shifting angles from 1° to 8°.

4. Finite Element Analysis of a Symmetrical Rotor

A variety of numerical methods are available for the analysis of electromagnetic torque. These include, the virtual work method, the Maxwell stress tensor method, the nodal force method, and the Coulomb virtual work method, which are all methods used to analyze the cogging torque of PMBLDC motors. For the determination of cogging torque, precise field solutions are required. That is to say that a sophisticated mesh discretization is vital in FEA analysis, just as a dependable physical model is crucial for analytical calculations.

This section describes the outcomes of the 3D FEA analysis of the examined PMBLDC motor with the symmetrical rotor. Cogging torque can be determined numerically using the FEA method. Without a prototype, FEA is a powerful and viable tool for defining the performance of a given design [27,28]. The main target of this work was to decrease the cogging torque by using the magnet displacement method.

A 12-slot, 4-pole PMBLDC motor was considered as the motor for which the cogging torque was determined analytically using the FEA method. Further, on the basis of the FEA analysis, a comparative study was performed to compare the effect of the magnet shifting with the symmetrical structure. Figure 5 shows the conventional rotor with symmetrical magnets. Table 3 shows the FEA results for the symmetrical structure.
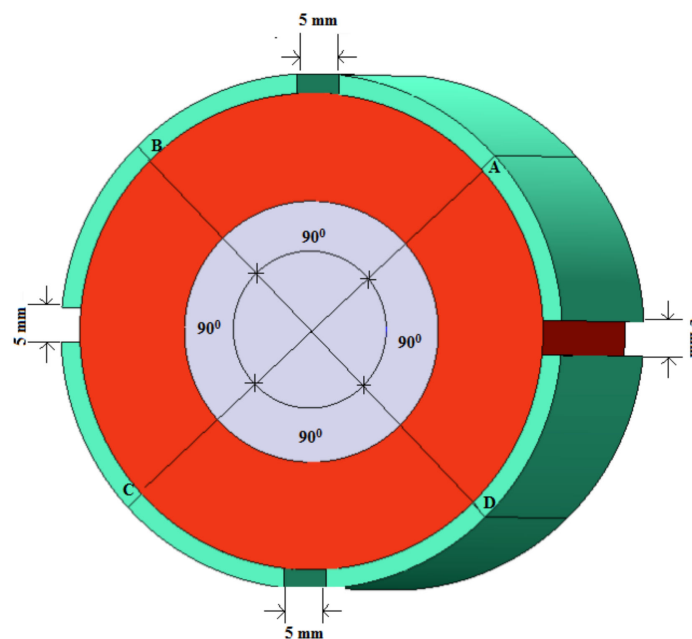
Figure 5. Conventional rotor with symmetrical magnets.

Table 3. FEA results for BLDC motor with symmetrical magnets.

Shifting Angle and Spacing between Permanent Magnets								Cogging Torque (Nm)
A-B		B-C		C-D		D-A		
Angle (°)	Space (mm)	Angle (°)	Space (mm)	Angle (°)	Space (mm)	Angle (°)	Space (mm)	
90	5	90	5	90	5	90	5	0.64

5. Effect of Angle Shift on Cogging Torque

In practice, magnet poles are neither made identically nor placed at the perfect location. There are a lot of methods available to obtain asymmetrical rotor structures. In this work, the method of shifting angle between the poles was adopted. Maintaining the L/τ ratio between 0.6 and 0.8, shifting angles were considered between 1° and 8°. From the analysis, it is understandable that the cogging torque is very sensitive to variations in the magnet angle. Figure 6 shows the procedure for finding the shifting angle with the minimum cogging torque.

In order to minimize cogging torque, a permanent magnet shift is considered here. A range of distinct angles were considered to analyze the effect of the angle shift on the rotor magnets. The permanent magnets on the rotor were shifted from 1° to 8°. The actual position of the permanent magnets was 90°. For every 1° change, four possible combinations were obtained. Table 4 shows the tabulation of the results of cogging torque with variation of magnet shifting from 1° to 8°. It shows that the shifting angle with 3° has the minimum cogging torque. The lowest cogging torque is 0.16 Nm when the angle between the poles A-B is 87°, B-C is 93°, C-D is 87° and D-A is 93°. Figure 7 shows the placement of the rotor magnet after applying the magnet shift to the rotor magnets. From the figure, it is clear that when the poles A, B, C, and D have a 90° difference with respect to each other, then each magnet has a 5 mm difference. Figure 7a shows shifting angle between the magnet is 1°. The spacing between A-B and C-D 4.44 mm and B-C and D-A is 5.56 mm. Figure 7b shows shifting angle between the magnet is 2°. The spacing between A-B and C-D is 5.58 mm and B-C and D-A is 4.42 mm. In Figure 7c the shifting angle between the magnet is 3°. The spacing between A-B and C-D is 3.32 mm and B-C and D-A is 6.68 mm. in Figure 7d the shifting angle between the magnet is 4°. The spacing between A-B and C-D is 7.24 mm and B-C and D-A is 2.76 mm. Figure 7e shows shifting

angle between the magnet is 5°. The spacing between A-B and C-D is 2.2 mm and B-C and D-A is 7.8 mm. Figure 7f shows shifting angle between the magnet is 6°. The spacing between A-B and C-D is 8. 38mm and B-C and D-A is 1.62 mm. In Figure 7g the shifting angle between the magnet is 7°. The spacing between A-B and C-D is 8.95 mm and B-C and D-A is 1.05 mm. When the shift angle becomes 8° in Figure 7h, the spacing between A-B and C-D is 9.52 mm, and the spacing between B-C and D-A is 0.48 mm. If we again increase the shift angle to 9°, the two magnets merge, and will act like a two-pole machine.
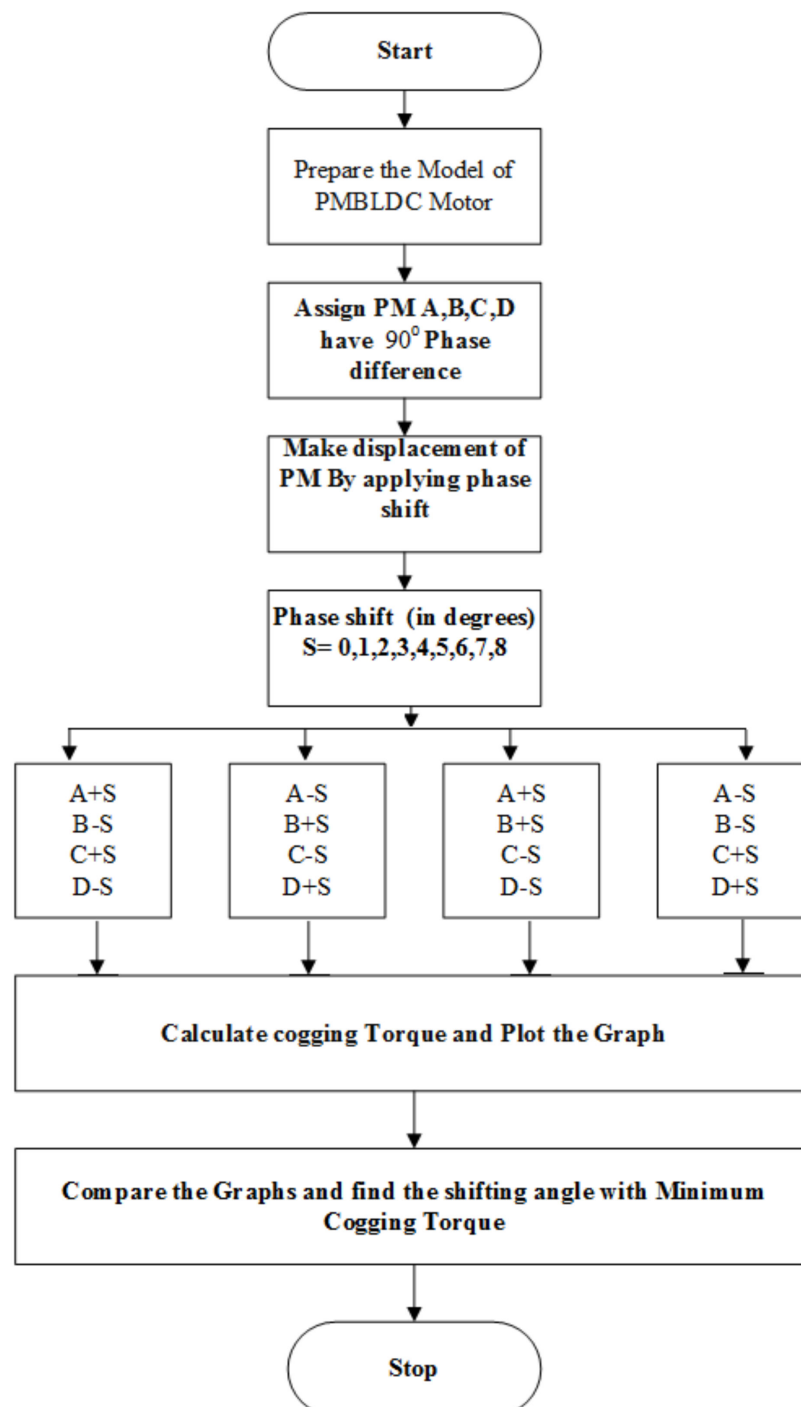
Figure 6. Flowchart for the procedure for finding shifting angle with minimum cogging torque.

Table 4. Tabulation of results of cogging torque with variation of magnet shifting from 1° to 8°.

| Shifting Angle (°) | Shifting Angle and Spacing between Permanent Magnets | | | | | | | | Cogging Torque (Nm) |
| | A-B | | B-C | | C-D | | D-A | | |
	Angle (°)	Space (mm)	Angle (°)	Space (mm)	Angle (°)	Space (mm)	Angle (°)	Space (mm)	
1°	91	5.56	89	4.44	91	5.56	89	4.44	0.64
	89	4.44	91	5.56	89	4.44	91	5.56	0.42
	89	4.44	89	4.44	91	5.56	91	5.56	0.41
	91	5.56	91	5.56	89	4.44	89	4.44	0.61
2°	92	5.58	88	4.42	92	5.58	88	4.42	0.89
	88	4.42	92	5.58	88	4.42	92	5.58	0.34
	88	4.42	88	4.42	92	5.58	92	5.58	0.82
	92	5.58	92	5.58	88	4.42	88	4.42	0.95
3°	93	6.68	87	3.32	93	6.68	87	3.32	0.48
	87	3.32	93	6.68	87	3.32	93	6.68	0.8
	87	3.32	87	3.32	93	6.68	93	6.68	0.16
	93	6.68	93	6.68	87	3.32	87	3.32	0.25
4°	94	7.24	86	2.76	94	7.24	86	2.76	1.2
	86	2.76	94	7.24	86	2.76	94	7.24	0.22
	86	2.76	86	2.76	94	7.24	94	7.24	0.56
	94	7.24	94	7.24	86	2.76	86	2.76	1.3
5°	95	7.8	85	2.2	95	7.8	85	2.2	2.1
	85	2.2	95	7.8	85	2.2	95	7.8	0.56
	85	2.2	85	2.2	95	7.8	95	7.8	0.5
	95	7.8	95	7.8	85	2.2	85	2.2	2.5
6°	96	8.38	84	1.62	96	8.38	84	1.62	1.7
	84	1.62	96	8.38	84	1.62	96	8.38	0.33
	84	1.62	84	1.62	96	8.38	96	8.38	0.39
	96	8.38	96	8.38	84	1.62	84	1.62	3.4
7°	97	8.95	83	1.05	97	8.95	83	1.05	2.9
	83	1.05	97	8.95	83	1.05	97	8.95	0.68
	83	1.05	83	1.05	97	8.95	97	8.95	1.5
	97	8.95	97	8.95	83	1.05	83	1.05	2.4
8°	98	9.52	82	0.48	98	9.52	82	0.48	2.1
	82	0.48	98	9.52	82	0.48	98	9.52	0.7
	82	0.48	82	0.48	98	9.52	98	9.52	0.56
	98	9.52	98	9.52	82	0.48	82	0.48	4

Table 5 shows the comparison of the 3D FEA results of cogging torque when shifting the magnetic pole angle from 1° to 8°. The graphical representation of variation in the cogging torque with magnet shifting is shown in Figure 8. From the above comparison, when the shifting angle is 3°, the lowest cogging torque of 0.16 Nm is obtained. The base rotor has a cogging torque of 0.64 Nm. Compared with the base rotor, the new asymmetrical rotor structure exhibits a 75% reduction in cogging torque.
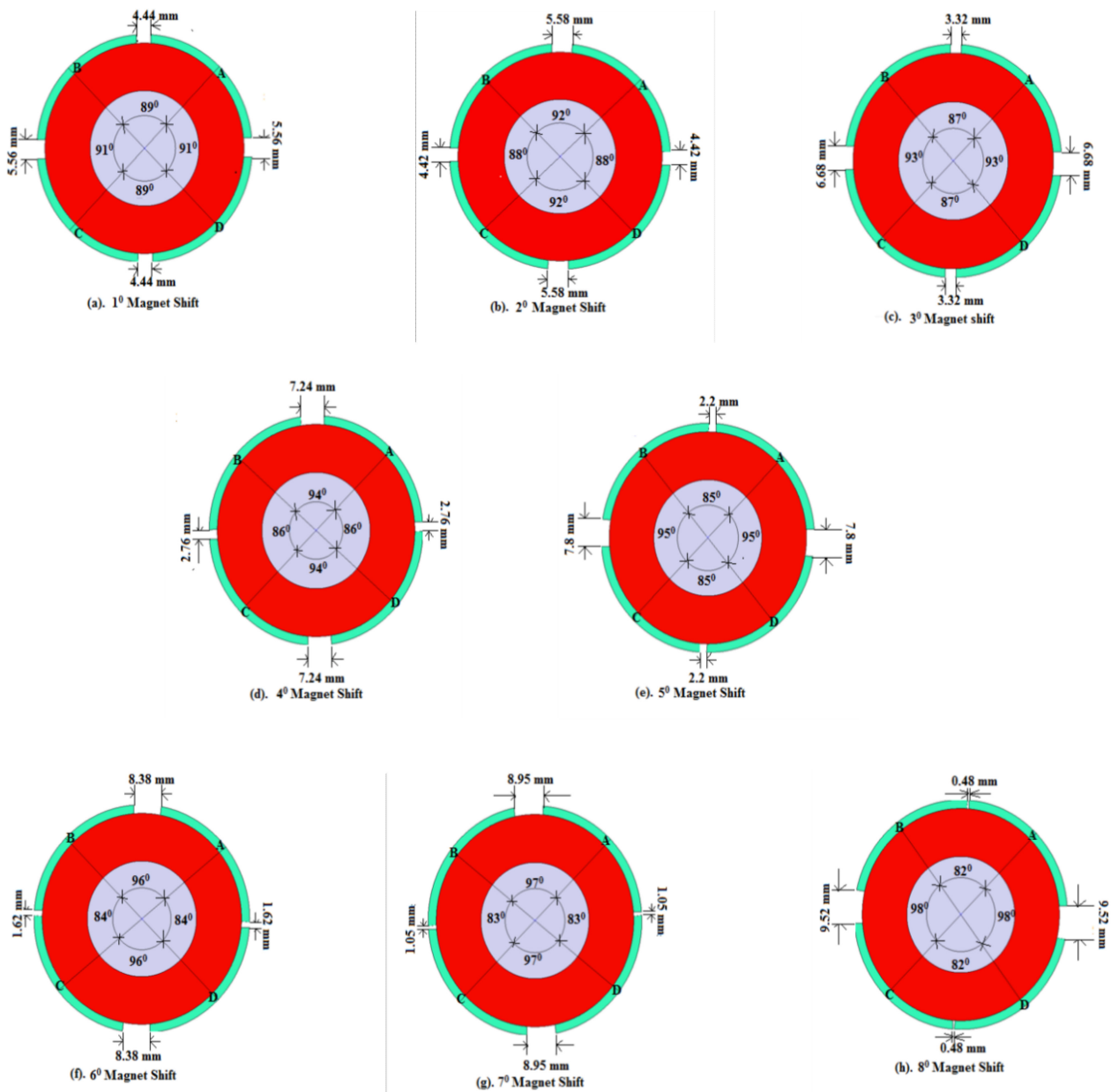
Figure 7. Rotor magnet shift from 1° to 8°.

Table 5. Comparison of 3D FEA results for cogging torque.

Sl. No.	Shifting Angle (°)	Angle between Magnets (°)				Cogging Torque (Nm)
		A-B	B-C	C-D	D-A	
1	1	89	91	89	91	0.41
2	2	92	88	92	88	0.34
3	3	87	93	87	93	0.16
4	4	94	86	94	86	0.22
5	5	85	95	85	95	0.5
6	6	96	84	96	84	0.33
7	7	97	83	97	83	0.68
8	8	82	98	82	98	0.56
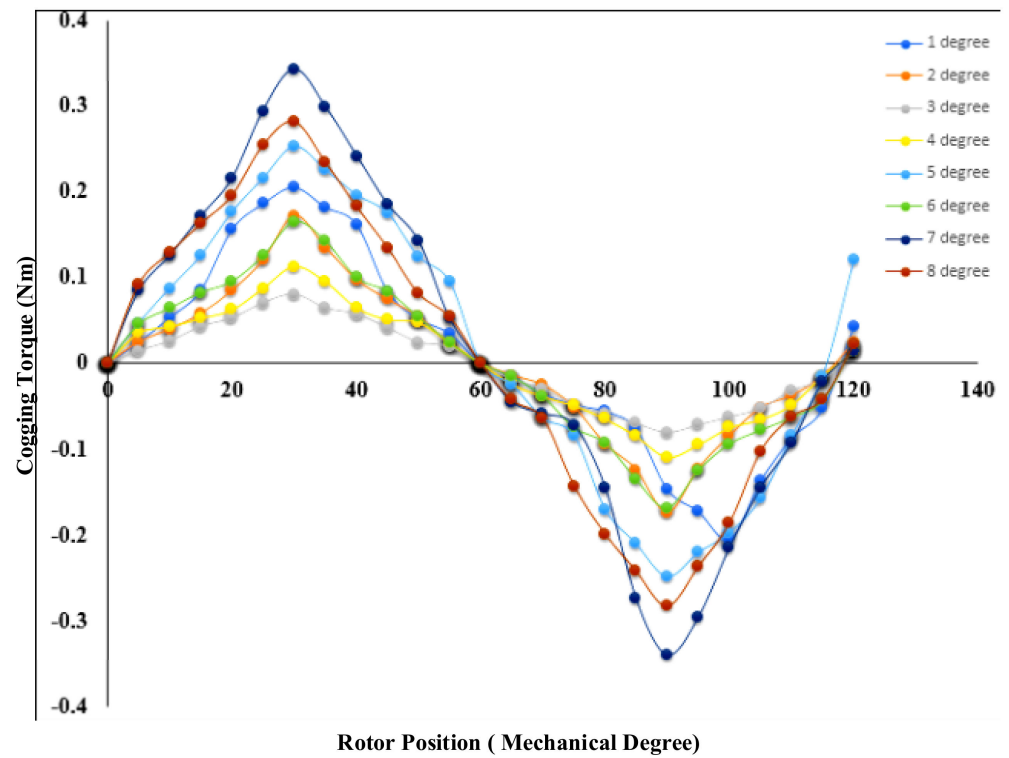
Figure 8. FEA results of cogging torque with varying shifting angle.

One of the main reasons for the existence of cogging torque is the change in magnetic flux density. Assessment of flux density and assessment of flux lines are two pivotal steps in FEA. Whenever the magnet displacement is applied to the rotor, the flux density is lower than that of the symmetrical structure. Though the flux density remains the same in many regions of the BLDC motor, the maximum flux density, indicated by yellow color, is attained in some parts of the stator (in addition to the permanent magnets). Red areas indicate undesirably high flux density, which may result in hot spots that could damage the motor. When applying magnet displacement in the rotor, the flux density decreases. This causes a reluctance to change that is comparatively better than the existing method, resulting in a reduction in cogging torque. Figures 9 and 10 show the flux plot distribution in symmetrical and asymmetrical rotors.
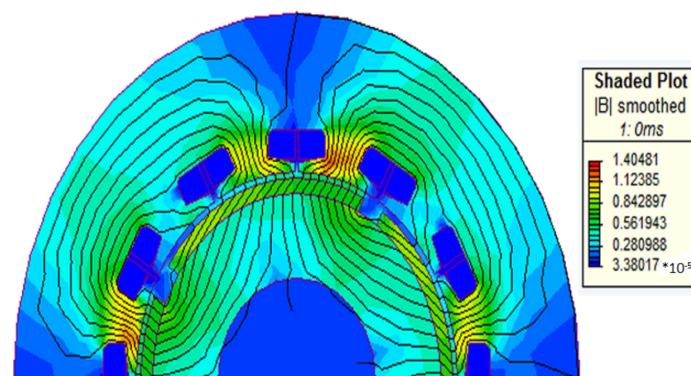

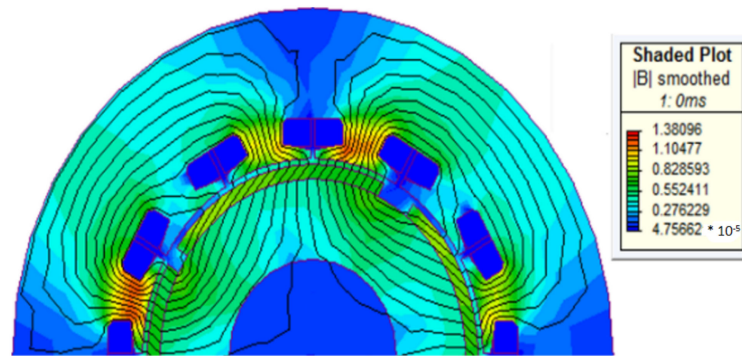**Figure 9.** Flux plots in symmetrical rotor.

Figure 10. Flux plots in the asymmetrical rotor.

Figure 11a shows the symmetrical rotor structure with an angle difference of 90°, Figure 11b shows the asymmetrical rotor structure with 3° magnet shifting. There is a small difference in the spacing of the permanent magnet. In the symmetrical design, all the rotor magnets are placed equally at a distance of 5 mm from one another, and in the asymmetrical structure, the spacing between magnets A and B is 3.32 mm, and the spacing between magnets B and C is 6.68 mm. Table 6 shows a comparison of the cogging torque between the symmetrical and asymmetrical rotors.
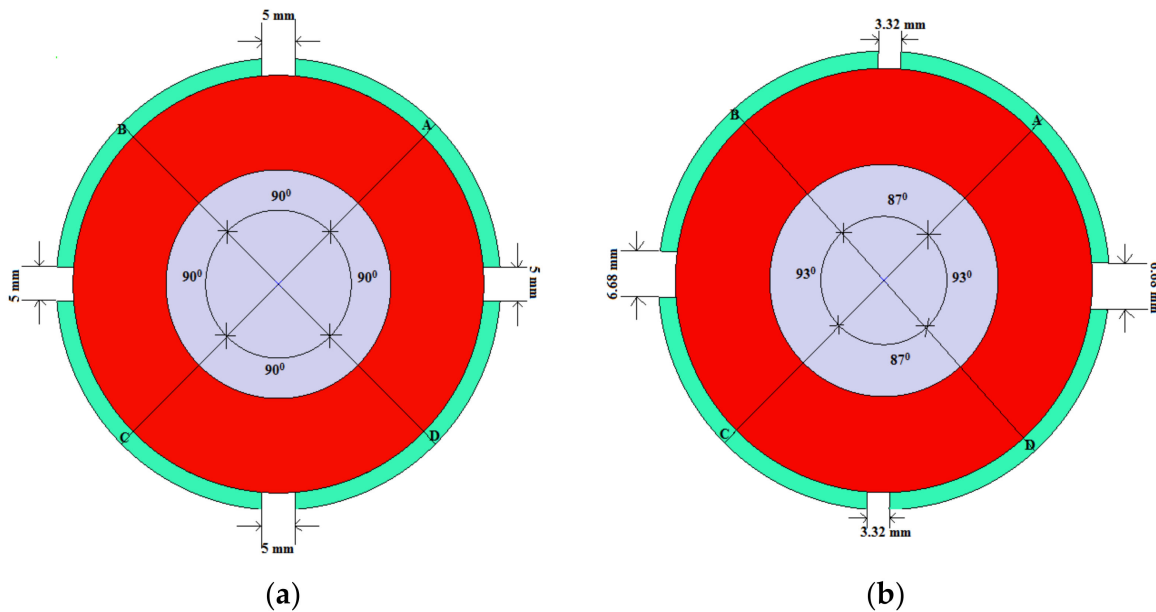

(a)   (b)

Figure 11. Compared Rotor structure (**a**) Symmetrical rotor structure with an angle difference of 90°; (**b**) asymmetrical rotor structure with 3° magnet shifting.

Table 6. Comparison of cogging torque for the symmetrical and the asymmetrical rotor.

| Rotor Type	Angle between Magnets (°)				Cogging Torque (Nm)
	A-B	B-C	C-D	D-A	
Symmetrical	90°	90°	90°	90°	0.64
Asymmetrical	87°	93°	87°	93°	0.16

Table 7 presents a comparison of cogging torque results between simulation and analytical method. When the shifting angle is 3°, both methods have almost the same results. Figure 12 shows a graphical representation of the FEA results and the analytical results.

Table 7. Comparison of simulation and analytical result.

Shifting Angle (°)	Cogging Torque (Nm)	
	Simulation Result	**Analytical Result**
1	0.41	0.39
2	0.34	0.3
3	0.16	0.15
4	0.22	0.18
5	0.5	0.45
6	0.33	0.2
7	0.68	0.6
8	0.56	0.51
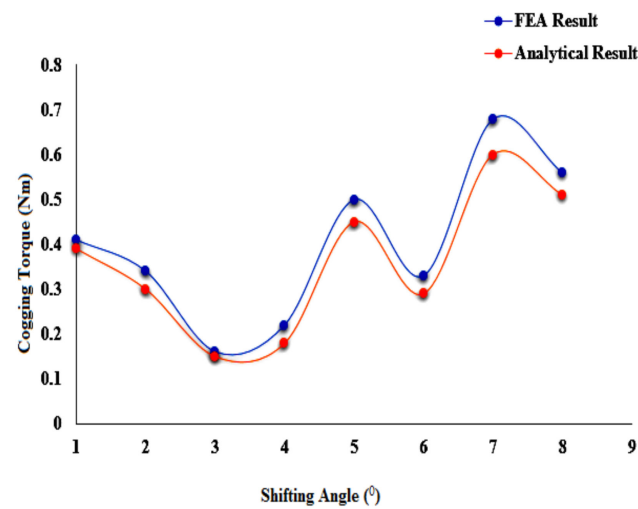
Figure 12. Comparison of FEA and analytical results.

The magnet shifting can reduce the cogging torque effectively without deteriorating the trapezoidal shape of the back-EMF. Figure 13 shows the back-EMF of the SPMBLDC motor with different magnet shifting angles. In this figure, 0° represents all four magnets being placed at an exactly 90° phase difference from one another, and is represented using blue color. The yellow color, which is very close and similar to the 0° case, phase shifts the back-EMF curve with a 3° phase shift
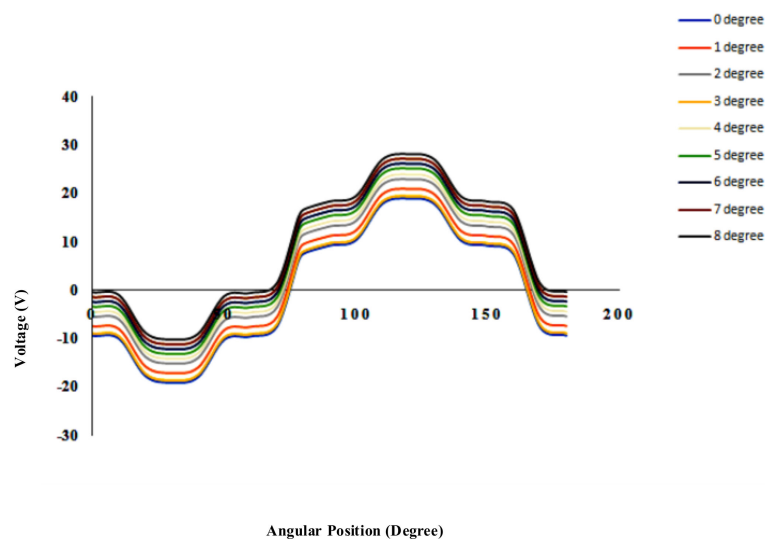
Figure 13. Comparison of back-EMF.

Figures 14–17 show the transient 3D results and the performance characteristics of symmetrical and asymmetrical rotor magnets. Even when the rotor magnetic angles are shifted, the acceleration of the BLDC motor is almost constant, and the initial speed is also maintained at a constant level, meaning that the speed of the BLDC motor increases linearly with respect to time. Figure 13 shows the time vs. speed characteristic of symmetrical and asymmetrical rotor magnets. Orange color represents the speed of the motor with the base model and blue color shows the speed of the motor with a 3-degree phase shift. From the figure, it is evident that the motor with a 3-degree phase shift is able to achieve greater speed than the base model within the specified time. Figures 14–16 present comparisons of the magnetic torque, load torque and net torque of the symmetrical magnet and the asymmetrical magnet. From the above figures, it is clear that the rotor with the 3-degree magnet shift has excellent torque vs. time characteristics when compared with the base model.
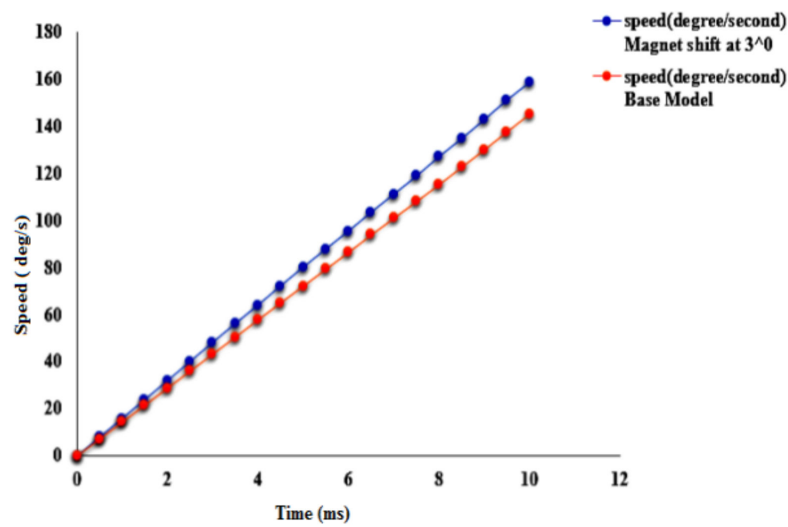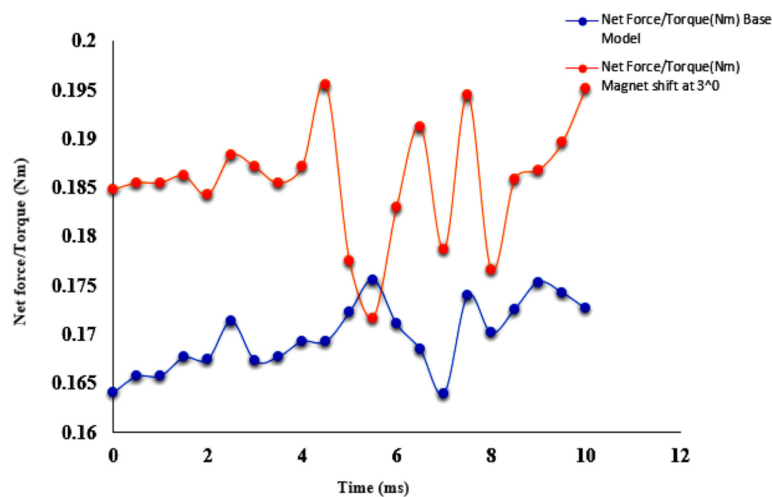

Figure 14. Speed vs. time.

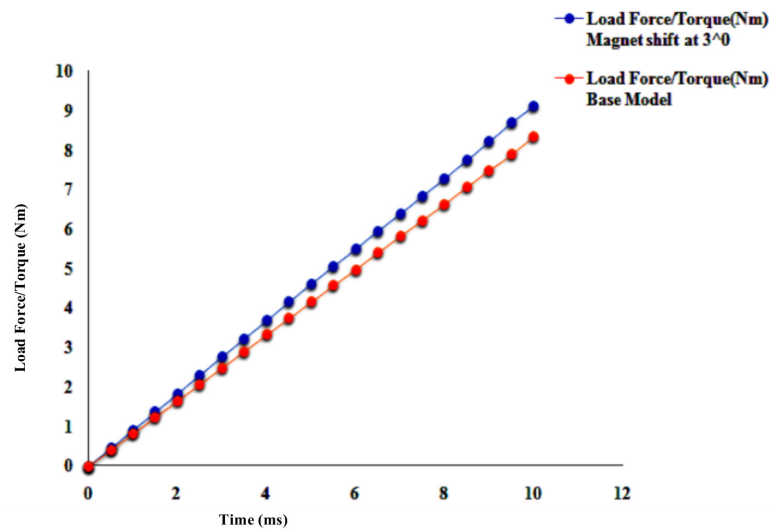**Figure 15.** Magnetic force/torque vs. time.
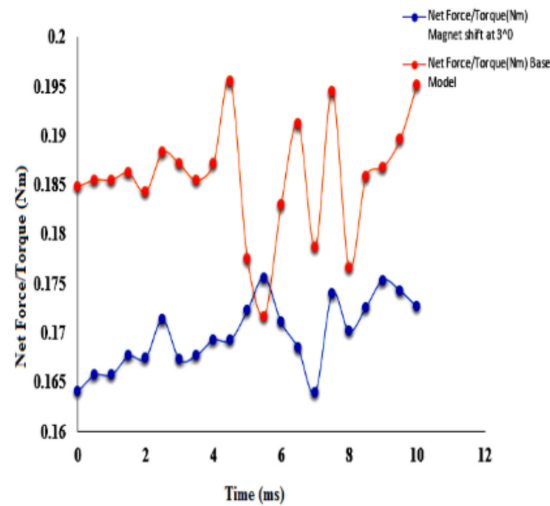
Figure 16. Load force/torque vs. time.

Figure 17. Load force/torque vs. time.

Figures 18 and 19 represent the cogging torque and the voltage under transient conditions. For cogging torque, the transient starts at 0.15 and increases to 0.45 Nm for a particular period before settling down to 0.16 Nm. Considering the transient scenario for voltage, it starts from 0 V and increases to 0.24 V, before after a particular period decreasing to 0.05 V and settling at 0.084 V.

In reference [29], in order to reduce cogging torque, a magnet shifting technique was adopted. The authors considered a 4 pole 12 slot machine. Table 8 shows the comparative results of the existing and proposed design.

Table 8. Comparative results of the existing and proposed design.

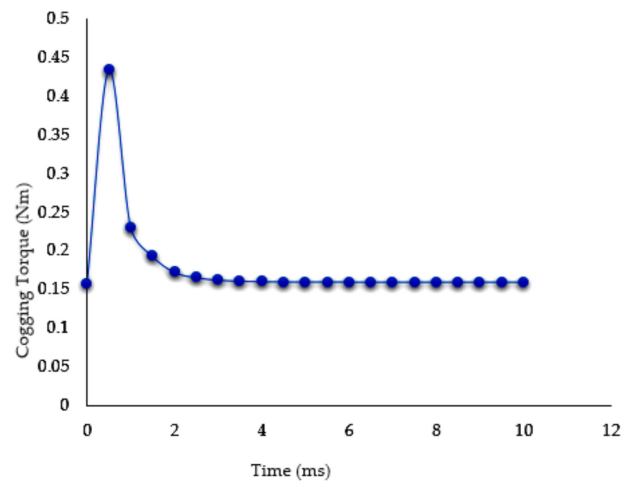| Parameters	Existing	Proposed
No. of slots	12	12
No. of Poles	4	4
Magnet shift angle	7.5°	3°
Pole arc	60°	63°
Cogging Torque	0.4 Nm	0.16 Nm

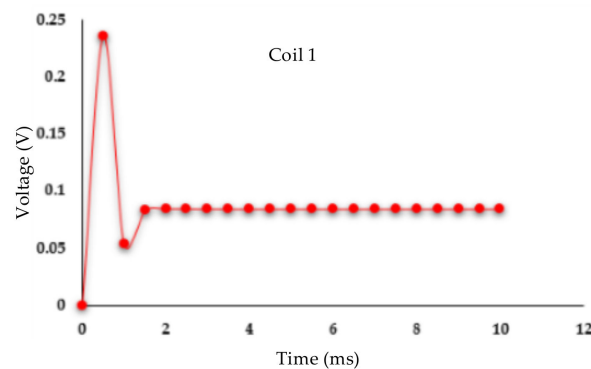**Figure 18.** Transient response of cogging torque.

Figure 19. Transient response of voltage.

On the basis of existing work, it is clear that the new proposed model offers a 60% reduction in cogging torque.

An undesirable effect that occurs in permanent magnet motors during shaft variation is torque ripple. This is a periodic increase and decrease in output torque. In BLDC motors, cogging torque is a crucial factor contributing to torque ripple. Figure 20 presents the resulting torque ripple waveform following a 3° magnetic shift. This is the difference between the maximum torque and the minimum torque compared to the average torque [30]. The rated torque of the motor was 1.424 Nm. The maximum, minimum and average values of electromagnetic torque were 1.18 Nm, 0.6 Nm and 1.1 Nm, respectively. Therefore, the degree of torque ripple was 52.7%.
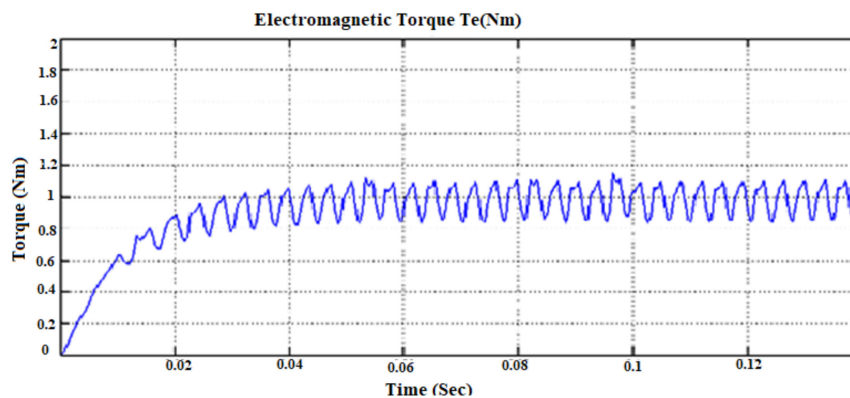

Figure 20. Torque ripple waveform with 3° magnetic shift.

6. Conclusions

A new method was proposed for the reduction of cogging torque in permanent magnet BLDC motors. In this method, a rotor with an asymmetrical magnet structure is recommended for the minimization of cogging torque. The asymmetry is achieved through the displacement of the permanent magnet. The shifting angle considered for the analysis was selected by maintaining the L/τ ratio within the permissible limit. Combinations from 1° to 8° were tried out. The magnet pole shifting caused variations in the flux line distribution and flux densities. The variation in flux density helped to achieve a reduction in cogging torque. When the shifting angle was 3°, the minimum cogging torque was obtained. The prototype adopted for this method was analyzed using FEA, showing an immense decrease in cogging torque. A novel analytical approach was also developed in order to be able to speculate regarding the effects on cogging torque in a permanent magnet BLDC motor. The predicted cogging torque curve showed good agreement with the FEA results. The proposed method is practical and capable of achieving low cogging torque. The proposed rotor structure with an asymmetrical magnet is advantageous for the minimization of cogging torque.

Author Contributions: T.A.A. and M.A.N.D. have same contribution in design in motor and article work. All authors have read and agreed to the published version of the manuscript.

Conflicts of Interest: The authors declare no conflict of interest.

Nomenclature

HP	Horse Power
Ph	Phase
η	Efficiency
P	No. of Poles
V	Supply Voltage
f	Frequency
Pf	Power factor
L	Stator Length
τ	Pole pitch
B_{av}	Specific magnetic Loading
ac	Specific electric Loading
Kw	Winding Factor
N	Speed
Q	kVA input
C_o	Output Coefficient
D	Stator Diameter
E_v	total energy variation
$E_{v.I}$	energy variation in iron
$E_{v.airgap}$	energy variation in airgap
$E_{v.PM}$	energy variation in PM
μ_0	permeability of air
B	magnetic flux density
α	angle of rotation of the rotor
l_m	length of the permanent magnet
l_g	length of airgap distribution
$B_{rs(\theta)}$	residual flux density along the periphery of the airgap
θ_s	Shifting angle
L_s	length of the stack
s	Slot number
R_r	Outer rotor diameter

References

1. Leitner, S.; Gruebler, H.; Muetze, A. Cogging Torque Minimization and Performance of the Sub-Fractional HP BLDC Claw-Pole Motor. *IEEE Trans. Ind. Appl.* **2019**, *55*, 4653–4664. [CrossRef]
2. Hannon, B.; Sergeant, P.; Dupre, L. Evaluation of the Torque in High-Speed PMSMs With a Shielding Cylinder and BLDC Control. *IEEE Trans. Magn.* **2018**, *54*, 1–8. [CrossRef]
3. Lee, M.; Kong, K.; Lee, M. Fourier-series-based Phase Delay Compensation of Brushless DC Motor Systems. *IEEE Trans. Power Electron* **2017**, *33*, 1. [CrossRef]
4. Kumar, B.A.; Kamal, C.; Amudhavalli, D.; Thyagarajan, T. Reformed Stator Design of BLDC Motor for Cogging Torque Minimization Using Finite Element Analysis. In *Proceedings of the 4th International Conference on Electrical Energy Systems (ICEES), Chennai, India, 7–9 February 2018*; Institute of Electrical and Electronics Engineers (IEEE): Chennai, India, 2018; pp. 481–484.
5. Nam, D.-W.; Lee, K.-B.; Pyo, H.-J.; Jeong, M.-J.; Yang, S.-H.; Kim, W.-H.; Jang, H.-K. A Study on Core Skew Considering Manufacturability of Double-Layer Spoke-Type PMSM. *Energies* **2021**, *14*, 610. [CrossRef]
6. Goryca, Z.; Różowicz, S.; Różowicz, A.; Pakosz, A.; Leśko, M.; Wachta, H. Impact of Selected Methods of Cogging Torque Reduction in Multipolar Permanent-Magnet Machines. *Energies* **2020**, *13*, 6108. [CrossRef]
7. Dini, P.; Saponara, S. Cogging Torque Reduction in Brushless Motors by a Nonlinear Control Technique. *Energies* **2019**, *12*, 2224. [CrossRef]
8. Dini, P.; Saponara, S. Design of an Observer-Based Architecture and Non-Linear Control Algorithm for Cogging Torque Reduction in Synchronous Motors. *Energies* **2020**, *13*, 2077. [CrossRef]
9. Sumega, M.; Rafajdus, P.; Stulrajter, M. Current Harmonics Controller for Reduction of Acoustic Noise, Vibrations and Torque Ripple Caused by Cogging Torque in PM Motors under FOC Operation. *Energies* **2020**, *13*, 2534. [CrossRef]
10. Doss, M.A.N.; Brindha, R.; Mohanraj, K.; Dash, S.S.; Kavya, K.M. A Novel Method for Cog-ging torque Reduction in Permanent Magnet Brushless DC Motor Using T-shaped Bifurcation in Stator Teeth. *Prog. Electromagn. Res. M* **2018**, *66*, 99–107. [CrossRef]
11. García-Gracia, M.; Romero, Á.J.; Ciudad, J.H.; Arroyo, S.M. Cogging Torque Reduction Based on a New Pre-Slot Technique for a Small Wind Generator. *Energies* **2018**, *11*, 3219. [CrossRef]
12. Hwang, M.-H.; Lee, H.-S.; Cha, H.-R. Analysis of Torque Ripple and Cogging Torque Reduction in Electric Vehicle Traction Platform Applying Rotor Notched Design. *Energies* **2018**, *11*, 3053. [CrossRef]
13. Kwon, J.-W.; Lee, J.-H.; Zhao, W.; Kwon, B.-I. Flux-Switching Permanent Magnet Machine with Phase-Group Concentrated-Coil Windings and Cogging Torque Reduction Technique. *Energies* **2018**, *11*, 2758. [CrossRef]
14. Liu, C.; Lu, J.; Wang, Y.; Lei, G.; Zhu, J.; Guo, Y. Techniques for Reduction of the Cogging Torque in Claw Pole Machines with SMC Cores. *Energies* **2017**, *10*, 1541. [CrossRef]
15. Doss, M.A.N.; Vijayakumar, S.; Mohideen, A.J.; Kannan, K.S.; Balaji Sairam, N.D.; Karthik, K. Reduction in Cogging torque and Flux per Pole in BLDC Motor by Adapting U-Clamped Magnetic Poles. *IJPEDS* **2017**, *8*, 297–304. [CrossRef]
16. Fazil, M.; Rajagopal, K.R. A Novel Air-Gap Profile of Single-Phase Permanent-Magnet Brushless DC Motor for Starting Torque Improvement and Cogging Torque Reduction. *IEEE Trans. Magn.* **2010**, *46*, 3928–3932. [CrossRef]
17. Hwang, S.-M.; Eom, J.-B.; Hwang, G.-B.; Jeong, W.-B.; Jung, Y.-H. Cogging torque and acoustic noise reduction in permanent magnet motors by teeth pairing. *IEEE Trans. Magn.* **2000**, *36*, 3144–3146. [CrossRef]
18. Park, Y.-U.; Cho, J.-H.; Kim, D.-K.; Young-Un, P. Cogging Torque Reduction of Single-Phase Brushless DC Motor with a Tapered Air-Gap Using Optimizing Notch Size and Position. *IEEE Trans. Ind. Appl.* **2015**, *51*, 4455–4463. [CrossRef]
19. Rahman, M.M.; Kim, K.-T.; Hur, J. Design and Optimization of Neodymium-Free SPOKE-Type Motor with Segmented Wing-Shaped PM. *IEEE Trans. Magn.* **2014**, *50*, 865–868. [CrossRef]
20. Han, K.-J.; Cho, H.-S.; Cho, D.-H.; Jung, H.-K. Optimal Core Shape Design for Cogging Torque Reduction of Brushless DC Motor Using Genetic Algorithm. *IEEE Trans. Magn.* **2000**, *36*, 4.
21. Hwang, K.-Y.; Rhee, S.-B.; Yang, B.-Y.; Kwon, B.-I. Rotor Pole Design in Spoke-Type Brushless DC Motor by Response Surface Method. *IEEE Trans. Magn.* **2007**, *43*, 1833–1836. [CrossRef]
22. Kim, H.-S.; You, Y.-M.; Kwon, B.-I. Rotor Shape Optimization of Interior Permanent Magnet BLDC Motor According to Magnetization Direction. *IEEE Trans. Magn.* **2013**, *49*, 2193–2196. [CrossRef]
23. Lee, S.-K.; Kang, G.-H.; Hur, J.; Kim, B.-W. Stator and Rotor Shape Designs of Interior Permanent Magnet Type Brushless DC Motor for Reducing Torque Fluctuation. *IEEE Trans. Magn.* **2012**, *48*, 4662–4665. [CrossRef]
24. Doss, M.A.N.; Jeevananthan, S.; Dash, S.S.; Jahir Hussain, M. Critical Evaluation of cogging torque in BLDC Motor with various Techniques. *Int. J. Autom. Control.* **2013**, *7*, 135–146. [CrossRef]
25. Doss, M.A.N.; Sridhar, R.; Karthikeyan, M. Cogging torque Reduction in Brushless DC Motor by Reshaping of Rotor Magnetic Poles with Grooving Techniques. *Int. J. Appl. Eng. Res.* **2015**, *10*, 36.
26. Zhenhong, G.; Liuchen, C.; Yaosuo, X. *Coggingtorqueof permanent Magnet Electric machines: An Overview*; IEEE: St. John's, NL, Canada, 2009; ISSN 0840–7789.
27. Chang, L.; Eastham, A.R.; Dawson, G.E. Permanent magnet Synchronous Motors: Finite Element Torque calculations. In Proceedings of the Conference Record of the IEEE Industry Applications Society Annual Meeting, San Diego, CA, USA, 1–5 October 1989; pp. 69–73.
28. Yang, Y.; Wang, X.; Zhang, R.; Ding, T.; Tang, R. The Optimization of Pole Arc Coefficient to Reduce Cogging torque in Surface-Mounted Permanent Magnet Motors. *IEEE Trans. Magn.* **2006**, *42*, 4.

29. Breton, C.; Bartolome, J.; Benito, J.A.; Tassinario, G.; Flotats, I.; Lu, C.W.; Chalmers, B.J. Influence of Machine Symmetry on Reduction of Cogging Torque in Permanent-Magne Brushless Motors. *IEEE Trans. Magn.* **2006**, *36*, 5.

30. Doss, M.A.N.; Mohanraj, K.; Kalyanasundaram, V.; Karthik, K. Reduction of Cogging Torque by Adapting Bifurcated Stator Slots and Minimization Of Harmonics And Torque Ripple in Brushless DC Motor. *Int. J. Power Electron. Drive Syst. (IJPEDS)* **2016**, *7*, 781. [CrossRef]